Quantifying the emission changes and associated air quality impacts during the COVID-19 pandemic in North China Plain: a response modeling study

Jia Xing[1,2], Siwei Li[3, 4, *], Yueqi Jiang[1,2], Shuxiao Wang[1,2,*], Dian Ding[1,2], Zhaoxin Dong[1,2], Yun Zhu[5], Jiming Hao[1,2]

[1] State Key Joint Laboratory of Environmental Simulation and Pollution Control, School of Environment, Tsinghua University, Beijing 100084, China

[2] State Environmental Protection Key Laboratory of Sources and Control of Air Pollution Complex, Beijing 100084, China

[3] School of Remote Sensing and Information Engineering, Wuhan University, Wuhan 430079, China

[4] State Key Laboratory of Information Engineering in Surveying, Mapping and Remote Sensing, Wuhan University, Wuhan 430079, China

[5] College of Environment and Energy, South China University of Technology, Guangzhou Higher Education Mega Center, Guangzhou 510006, China

[*]Corresponding Authors: Shuxiao Wang (email: shxwang@tsinghua.edu.cn; phone: +86-10-62771466; fax: +86-10-62773650); Siwei Li (email: siwei.li@whu.edu.cn)

Abstract

Quantification of emission changes is a prerequisite for the assessment of control effectiveness in improving air quality. However, the traditional bottom-up method for characterizing emissions requires detailed investigation of emissions data (e.g., activity and other emission parameters) that usually takes months to perform and limits timely assessments. Here we propose a novel method to address this issue by using a response model that provides real-time estimation of emission changes based on air quality observations in combination with emission-concentration response functions derived from chemical transport modeling. We applied the new method to quantify the emission changes in the North China Plain (NCP) due to the COVID-19 pandemic shutdown, which overlapped the Spring Festival holiday. Results suggest that the anthropogenic emissions of NO_2, SO_2, VOC, and primary $PM_{2.5}$ in NCP were reduced by 51%, 28%, 67% and 63%, respectively, due to the COVID-19 shutdown, indicating longer and stronger shutdown effects in 2020 compared to the previous Spring Festival holiday. The reductions of VOC and

primary $PM_{2.5}$ emissions are generally effective in reducing O_3 and $PM_{2.5}$ concentrations. However, such air quality improvements are largely offset by reductions in NO_x emissions. NO_x emission reductions lead to increases in O_3 and $PM_{2.5}$ concentrations in NCP due to the strongly VOC-limited conditions in winter. A strong NH_3-rich condition is also suggested from the air quality response to the substantial NO_x emission reduction. Well-designed control strategies are recommended based on the air quality response associated with the unexpected emission changes during the COVID-19 period. In addition, our results demonstrate that the new response-based inversion model can well capture emission changes based on variations in ambient concentrations, and thereby illustrate the great potential for improving the accuracy and efficiency of bottom-up emission inventory methods.

Keywords: emission changes, response model, ozone, $PM_{2.5}$, control effectiveness

1. Introduction

Accurate estimation of anthropogenic emissions is crucial for atmospheric modeling studies and provides the basis for developing effective air pollution controls (Wang et al., 2010). A comprehensive emission inventory consists of the emission rates of primary particulate matter components and gaseous pollutants and precursors that are allocated over time and space. These inventories are usually developed using bottom-up methods that gather detailed information about source activity and other emission parameters (Wang et al., 2011; Xing et al., 2015; Li et al., 2017). The challenge is that such investigation is costly and time consuming, and therefore the latest emission inventories usually lag current conditions by a year or more. Many studies also apply a top-down methods to constrain emission estimates using satellite retrievals and modeling methods (Tang et al., 2013, 2019; Lu et al., 2015; Miyazaki et al, 2017; Cao et al., 2018; Zhang et al., 2018). In general, the traditional top-down inversion methods use four-dimensional data assimilation (Mendoza-Dominguez and Russell, 2000) or Kalman Filter methods (Hartley and Prinn, 1993) combined with sensitivity analysis of chemical transport modeling, like decoupled direct method in three dimensions (Napelenok et al., 2008), or adjoint method (Cao et al., 2018), to optimize the gap between the simulation and observation through adjusting the emission from a priori estimate. The top-down inversion method can well reflect the change in emissions in a timely manner, and thus efficiently estimate emissions at high spatial and temporal resolution to complement bottom-up inventories. Previous inversion studies have focused on individual pollutants that can be measured directly; however, studies are lacking that use top-down methods to estimate emissions of multiple pollutants, including those that cannot be directly measured, such as primary fine particular matter (p-$PM_{2.5}$).

The ongoing Coronavirus disease 2019 (COVID-19) pandemic has led to 4,600 deaths in mainland China (by May 24, 2020, https://news.google.com/covid19/), and has resulted in a dramatic curtailment of routine economic and social activities. The shutdown of human activities during the COVID-19 pandemic has led to reduced pollutant emissions and possibly improved air quality (Shi et al., 2020; Wang

et al., 2020a). Yet according to ambient concentration measurements, heavy $PM_{2.5}$ pollution still occurred during the COVID-19 period, and formation of secondary pollutants was actually enhanced in China (Li et al., 2020; Huang et al., 2020). Some studies attributed pollution enhancements to atypical weather conditions that are favorable for air pollution formation (Wang et al., 2020b). Meanwhile, the unexpected reduction of anthropogenic emissions due to the COVID-19 shutdown might vary significantly for different sectors and species. For example, emissions from domestic sources might have increased due to a greater demand for home heating and other essential consumptions during periods with stay-at-home orders in effect. Moreover, the coincidence of the COVID-19 shutdown and the Spring Festival in China resulted in large numbers of people confined to their rural or small-city hometowns, where consumption patterns differ greatly from their primary residence in megacities. Relative to previous years, both emissions and meteorological conditions varied simultaneously during the 2020 COVID-19 shutdown, and an accurate estimation of the changes in anthropogenic emissions accounting for meteorological variations is needed to characterize the impacts of COVID-19 on air quality.

Here we propose a novel inversion technique based on a multi-pollutant nonlinear response model to estimate the emission changes in NCP during the COVID-19 shutdown. Emission changes for the COVID-19 period are calculated as the difference between emission estimates for actual conditions and hypothetical conditions assuming the shutdown did not occur. The hypothetical emissions are determined by combining top-down emission estimates from before and after the shutdown with estimates of the temporal variation in emissions from a bottom-up emission inventory. Additionally, we estimate the change in emissions associated with the Spring Festival holiday in 2019 to contrast with results for the combined Spring Festival holiday and COVID-19 shutdown in 2020. Finally, we evaluate the impacts on $PM_{2.5}$ and O_3 concentrations of the combined emission changes and for each emitted species to provide insights for the design of effective control strategies in the future.

2. Methods

2.1 Response model to estimate the actual emissions from observed surface concentrations

The principle of the new response-based inversion model (hereafter "the response model") is to adjust the assumed prior emissions such that concentration predictions match observations. Different from previous top-down methods that applying sensitivity based optimization, this study adopted emission-concentration response functions which provide real-time estimates of the concentrations under various emission scenarios. Therefore it can make the adjustment of emissions match with the observation more straightforwardly by avoiding the calculation of the sensitivities. Meanwhile, the natural linkage exists in air pollutants like $PM_{2.5}$ and O_3 since both pollutants have contributions from common precursors (NO_x and VOC), similar atmospheric diffusion/advection transport, and chemical oxidation reactions. The advantage of the new method is for its ability in representing the nonlinearity of $PM_{2.5}$ and O_3 to their precursor emissions, thus can assimilate both pollutants simultaneously by keeping the natural linkage. In addition, to address the "ill-posedness" inversion problem, we took advantage of all available observations for multiple pollutants, and constrained the adjustment of emissions at provincial scale rather than at each single grid cell. That means we only change of total emissions of each province but keep spatial and temporal variation the same as that in the priori emissions. Such design makes the new method has small sensitivity to the change of observation sites due to the use of prior knowledge of the spatial distribution of emissions, which is particularly useful for certain period when observations are not always available across the whole region. However, the new method has limited ability to assimilate concentrations at the edge of the control region, and may suffer uncertainties in the spatial and temporal variations which are unable to be adjusted by this method (Xing et al., submitted). Nevertheless, since the study mainly focuses on the relative change of total emissions over the NCP region due to the COVID-19 rather than improving the baseline emissions, thus our new method is more suitable to address such specific purpose.

The core element of the inversion method is a nonlinear response surface model (RSM) that

represents the emission-concentration response functions. The framework of the response model is illustrated in Figure 1. We conduct chemical transport model simulations using prior emissions to get the original simulated concentrations of six pollutants (i.e., NO_2; O_3; SO_2; $PM_{2.5}$; sulfate, SO_4^{2-}; and nitrate, NO_3^-), as well as the response functions derived from the RSM (Xing et al., 2011; Wang et al., 2011; Xing et al., 2017; 2018). We then adjust the total emission ratio of five pollutants (i.e., NO_2, VOC, SO_2, NH_3 and primary $PM_{2.5}$) in five provinces of NCP (i.e., Beijing, Tianjin, Hebei, Shandong, and Henan) to estimate the updated simulated concentrations to match with the observations. Since the RSM was originally built based on the 3-D chemical transport model through multiple-emission scenarios by changing total emissions at controlled regions, both local source and non-local transport and transformation have been considered in the assimilation.

Based on our previous knowledge of emission-concentration response relationships, we first adjust NO_x emissions such that RSM predictions match NO_2 observations (see E1), since NO_2 concentrations have a strong linear relationship with NO_x emissions (Xing et al., 2017).

$$E'_{NOx} = r_{NOx} \times E^*_{NOx} = E^*_{NOx} \times \frac{C^o_{NO2}}{C^s_{NO2}} \quad \text{(E1)}$$

where E'_{NOx} is the adjusted NO_x emissions; E^*_{NOx} is the prior NO_x emissions; r_{NOx} is the adjustment ratio for NO_x emissions; C^o_{NO2} is the observed NO_2 concentrations; and C^s_{NO2} is the simulated NO_2 concentrations.

Next, we adjust VOC emissions such that RSM predictions match observed O_3 concentrations, since O_3 concentrations are solely determined by VOC emissions after NO_x emissions are determined in the previous step. The adjusted VOC emission ratio (i.e., $r_{VOC} = E'_{VOC}/E^*_{VOC}$) is determined by solving the following equation E2:

$$\Delta O_3 = (C^o_{O3} - C^s_{O3}) = RSM_{O3}(r_{NOx}, r_{VOC}) \quad \text{(E2)}$$

where E'_{VOC} is the adjusted VOC emissions; E^*_{VOC} is the prior VOC emissions; ΔO_3 is the difference between observed O_3 concentrations (C^o_{O3}) and simulated O_3 concentrations (C^s_{O3}); and RSM_{O3} is the

response function of O_3 concentrations to NO_x and VOC emissions.

Although SO_2 concentrations are linearly related to SO_2 emissions, the chemical transport model overestimates SO_2 concentrations and underestimates SO_4^{2-} concentrations due to large uncertainties in simulating the rapid conversion of SO_2 to SO_4^{2-} during haze episodes (Zhang et al., 2019). To address this deficiency, we adjusted the SO_2 emissions using the observed SO_4^{2-}/SO_2 ratio such that the RSM predictions matched both the observed SO_2 and SO_4^{2-} concentrations. Since SO_4^{2-} concentrations are quite linearly related to SO_2 emissions when NH_3 emissions are at moderate levels (Wang et al., 2011), we assume that the unaccounted for SO_2-to-SO_4^{2-} conversion pathway contributes to differences in the observed and simulated SO_4^{2-}/SO_2 ratios. Under this assumption, simulated SO_2 concentrations are overestimated by the same ratio (α) that secondary SO_4^{2-} (C_{s-SO4}^{s}) concentrations are underestimated (see E3 and E4). The primary SO_4^{2-} concentration (C_{p-SO4}^{s}) was removed from the total SO_4^{2-} concentration in these calculations, because primary SO_4^{2-} is directly emitted and not related to the conversion of SO_2 to SO_4^{2-} (see E4).

$$C_{SO2}^{o} = \frac{1}{\alpha} \times r_{SO2} \times C_{SO2}^{s} \quad \text{(E3)}$$

$$C_{SO4}^{o} = \alpha \times r_{SO2} \times C_{s-SO4}^{s} + C_{p-SO4}^{s} \quad \text{(E4)}$$

$$\alpha = \left(\frac{C_{SO2}^{o}}{C_{SO4}^{o} - C_{p-SO4}^{s}} \Big/ \frac{C_{SO2}^{s}}{C_{SO4}^{s}} \right)^{1/2} \quad \text{(E5)}$$

The adjusted SO_2 emission ratio (r_{SO2}) is estimated by taking the ratio of observed SO_2 (C_{SO2}^{o}) to simulated SO_2 (C_{SO2}^{s}) multiplied by α, which accounts for the model deficiency in simulating the rapid conversion of SO_2 to SO_4^{2-}. For simplification, here we estimate the α value at a domain and temporal averaged level (i.e., identical across the space and time), though such ratio might vary with time and space. Also the primary SO_4 concentrations were assumed to be correct. The α is smaller than 1 because the observed SO_4^{2-}/SO_2 is usually greater than the simulation. The inclusion of the α may help the response model avoid the underestimation of SO_2 emissions.

Using the adjusted NO_x, VOC, and SO_2 emissions from previous steps, we next adjusted NH_3 emissions such that RSM predictions of NO_3^- concentrations matched observations:

$$\Delta NO_3^- = (C_{NO3}^o - C_{NO3}^s) = RSM_{NO3}(r_{NOx}, r_{VOC}, r_{SO2}, r_{NH3}) \quad \text{(E6)}$$

where $r_{NH3} = E'_{NH3}/E^*_{NH3}$, E'_{NH3} is the adjusted NH_3 emissions, and E^*_{NH3} is the prior NH_3 emissions.

After updating the emissions of the four gaseous precursors, the secondary portion of $PM_{2.5}$ was correspondingly determined, including the secondary organic aerosol contributed by the VOC emissions. Finally, the primary $PM_{2.5}$ emissions were adjusted to provide agreement between simulated and observed total $PM_{2.5}$ concentrations:

$$\Delta PM_{2.5} = (C_{PM2.5}^o - C_{PM2.5}^s) = RSM_{PM2.5}(r_{NOx}, r_{VOC}, r_{SO2}, r_{NH3}, r_{p-PM2.5}) \quad \text{(E7)}$$

where $r_{p-PM2.5} = E'_{p-PM2.5}/E^*_{p-PM2.5}$, $E'_{p-PM2.5}$ is the adjusted primary $PM_{2.5}$ emissions, and $E^*_{p-PM2.5}$ is the prior primary $PM_{2.5}$ emissions.

The prior emissions used here were based on a bottom-up inventory developed for 2017. Since our study focuses on periods in 2019 and 2020, we first use the response model to adjust the 2017 emission inventory to match the observations during two study periods. The first study period was defined as 1 January – 31 March 2019 to capture changes in activity due the Spring Festival. The second study period was defined as the same three months in 2020 to capture the COVID-19 shutdown in NCP, which overlapped the 2020 Spring Festival holiday. We defined three sub-periods within the three months in each year as pre-shutdown (Period 1), shutdown (Period 2), and post-shutdown (Period 3). The days selected for sub-periods differed in 2019 and 2020 due to differences in the dates and lengths of the shutdowns. For 2019, we defined Period 1: 1–29 Jan. (29 days); Period 2: 30 Jan. – 18 Feb. (20 days), which is a week before and after the 2019 Lunar New Year holidays; and Period 3: 19 Feb. – 31 Mar. (41 days). For 2020, we defined Period 1: 1–22 Jan. (22 days); Period 2: 23 Jan. – 5 Mar. (33 days), which is from the date that Chinese authorities began targeted transportation shutdowns until all human activities began recovering in early March (http://www.gov.cn/index.htm); and Period 3: 6–31 Mar. (26 days). The stage-averaged

emissions are corrected by applying a unified change ratio to each pollutant emission at each stage, and the temporal variations such as hourly profiles are kept the same as those in the priori estimates.

The RSM was developed using ambient concentrations from simulations with the Community Multiscale Air Quality (CMAQ, version 5.2.1) model, which incorporated meteorological fields from the Weather Research and Forecasting (WRF, version 3.8) model. The WRF-CMAQ system was configured as in our previous studies, and model performance for meteorological variables and pollutant concentrations was evaluated (Ding et al., 2019). The RSM was developed following the same design as our previous study (Xing et al., 2017), in which the polynomial response functions for O_3, $PM_{2.5}$ and $PM_{2.5}$ components were fitted by 40 brute-force CMAQ simulations. Specifically, deep-learning technology was used to fit response surfaces for the three months in 2019 and 2020 using CMAQ simulations for baseline and zero-out emissions conditions (see Figure 2 in Xing et al. (2020)). The response surfaces were developed using year-specific meteorology based on WRF simulations to account for differences in meteorological conditions between 2019 and 2020.

Measurements of ambient concentrations of NO_2, SO_2, O_3 and $PM_{2.5}$ were obtained from the China National Environmental Monitoring Centre (http://106.37.208.233:20035/). Measurements of $PM_{2.5}$ chemical components, including NO_3^- and SO_4^{2-}, were provided by the urban PM data analysis platform in the 2+26 cities of Beijing-Tianjin-Hebei and surrounding regions (http://106.37.181.120:9011/bfs). All monitoring data were given as hourly-averaged concentrations at the monitoring sites shown in Figure 2. As in our previous RSM studies, daily daytime O_3 concentrations were analyzed based on afternoon averages (12:00pm-6:00pm local time), and $PM_{2.5}$ concentrations were based on daily 24-hour averages (Xing et al., 2018). Only data at monitoring sites that covered the 90% of entire period is considered. Since the monitors sample pollutants at discrete locations and measurements are not available for all days at all sites, provincial average concentrations were used to facilitate adjustments domain-wide for all days in each study period. The provincial average concentrations were calculated using spatially and temporally

matched simulated and observed values.

2.2 Hypothetical emissions without shutdown effects

The actual emissions can be derived using observed concentrations and the response model. However, hypothetical emissions under the assumption of no shutdown effects are also needed to estimate the changes in emissions due to the 2019 and 2020 shutdowns. We estimate the hypothetical emissions using the temporal profiles of sectoral emissions from the bottom-up inventory in combination with the derived (actual) emissions for the pre- and post-shutdown periods. We assume that the Spring Festival shutdowns in 2019 have negligible influence on emissions during the periods before and after the shutdown (i.e., Period 1 and Period 3, respectively), while the COVID-19 pandemic in 2020 might have had lag effects after the shutdown due to reduced economic activity or relaxed pollutant controls. However, we concentrate our analysis of COVID-19 impacts on emissions and air quality in the official shutdown period only (Period 2). The hypothetical no-shutdown emissions for Period 2 (noted as Period 2H) are estimated using ratios of emissions for Period 2 and Period 1 and 3 based on the temporal profile (i.e., reflect the monthly variation across a year) of the bottom-up inventory which only reflects the natural evolution of emissions across a year for each sector. It is roughly close to the temporally averaged ratios between the Period 1 and 3, and the exact values depend on the number of days covering in each period. This approach develops hypothetical emissions following the typical variation in emissions without shutdown effects. Note that we use the temporal profile to determine the change in Period 2 emissions relative to Period 1 and 3, and so emissions from both Period 1 and 3 are needed to estimate Period 2H emissions.

The emission changes due to the COVID-19 shutdown can be estimated by taking the difference of emissions in Period 2, derived from the response model, and emissions in Period 2H, estimated from emissions in Period 1 and 3 using the temporal profile of bottom-up sectoral emissions. The impacts of emission changes during the COVID-19 shutdown on $PM_{2.5}$ and O_3 concentrations are then estimated with

the RSM. In addition to the combined impacts of emission changes from multiple species, we estimate the impacts of individual pollutant emissions on $PM_{2.5}$ and O_3. Due to the nonlinearity of emission-concentration response functions, the impacts of individual pollutant emissions can vary significantly when other pollutant emissions are change simultaneously (Xing et al., 2018). To simplify the evaluation, we define an incremental method for analyzing the individual pollutant impacts in this study by adding incremental changes in pollutant emissions to the previous simulation in the following order: NO_x, VOC, NH_3, SO_2 and primary $PM_{2.5}$, as described in Table 1. The impacts of individual pollutant emissions on O_3 and $PM_{2.5}$ concentrations are then estimated from the difference between the incrementally adjusted simulation and the previous one. Note that this approach is an approximation, and the impacts of individual pollutants could change if a different order is used.

3. Results

3.1 Emission changes due to the shutdown

Using the response model, the daily emissions of NO_x, VOC, NH_3, SO_2 and primary $PM_{2.5}$ in NCP are estimated for three periods in 2019 and 2020, as summarized in Figure 3 and detailed in Table 2 by provinces.

For Period 1 before the activity disruptions, the emissions of NO_x, SO_2, and VOC in NCP decreased by 11%, 25%, and 8% between 2019 and 2020, respectively. These reductions reflect the progress of air pollution controls between 2019 and 2020, and demonstrate the ability of the model to capture emission changes from routine air pollution control actions. The p-$PM_{2.5}$ emissions also significantly decreased in Beijing-Tianjin-Hebei provinces but increased in Shandong and Henan. The NH_3 emissions did not change during this two-year period, since NH_3 is not considered in current policies.

Activity reductions occurred in Period 2 in both 2019 and 2020, although the shutdown due the Spring Festival in 2019 is much shorter than the COVID-19 shutdown in 2020. The emissions of NO_x, SO_2 and p-$PM_{2.5}$ in Period 2 in 2020 are substantially lower than in 2019 (29%, 22% and 73%,

254 respectively). The decreases of NO_x and p-$PM_{2.5}$ for Period 2 between 2019 and 2020 are larger than the
255 decreases for Period 1, which did not experience shutdowns. Such results suggest that the COVID-19
256 shutdown in 2020 had longer and stronger impacts on emissions than the Spring Festival shutdown in
257 2019. Interestingly, emissions of NH_3 and VOC increased significantly (by 5% and 14%) from 2019 to
258 2020 in Period 2. These changes are likely due to the temporal variations of emissions of both species,
259 which are enhanced in warmer months due to stronger evaporation. Period 2 in 2020 extended farther into
260 the Spring (until early March) than Period 2 in 2019, and thus led to increased evaporative emissions of
261 NH_3 and VOC. These results also demonstrate the importance of developing emissions with high temporal
262 resolution.

263 For Period 3 after the shutdown, the decreases of NO_x emissions (14%) are similar to those in Period
264 1 (11%), indicating the recovery of the activity. However, the emissions of VOC and p-$PM_{2.5}$ are much
265 lower in Period 3 in 2020 compared to that in 2019, suggesting the lag effects after the COVID-19
266 shutdown in 2020. In contrast, the small increases of SO_2 emissions in 2020 (2%) might be associated
267 with the extended central heating activity through the end of March in 2020, compared with mid-March
268 in 2019. Higher NH_3 emissions in Period 3 in 2020 than 2019 are also due to the larger coverage of warm
269 days in Period 3 of 2020. NH_3 emissions show the strongest monthly variations among all pollutants
270 (Figure 3). Similarly, increases in VOC emissions are also driven by the change of meteorological
271 conditions (i.e., the higher air temperature in March leads to a larger evaporative emissions), though the
272 growth of VOC emissions from Period 1 to Period 3 is reduced by the COVID-19 shutdown in 2020. Such
273 results also demonstrate that the response model can capture the temporal variations of emissions even in
274 cases where emissions are strongly coupled with meteorological conditions.

275 The influence of the shutdown is estimated as the difference in emissions between Period 2H
276 (hypothetical emissions without shutdown effects) and Period 2 (actual emissions), as shown in Figure 3
277 (grey and red bars respectively) and detailed in Table 3 by NCP province. Due to the COVID-19 shutdown

278 in 2020, emissions of NO_x, VOC and $PM_{2.5}$ decreased substantially by 51%, 67% and 63%, respectively.
279 SO_2 emissions also decreased by 28%, while NH_3 emissions experienced very small increases (+2%)
280 which might be associated with increased activities in rural areas (e.g., potential NH_3 emission sources
281 like stool burning) as many people relocated from megacities to small towns or the countryside. Compared
282 to the effects of the Spring Festival in 2019, the COVID-19 shutdown led to greater reductions in NO_x,
283 SO_2 and $PM_{2.5}$ emissions. The smaller VOC reduction in 2020 compared to 2019 might be due to the
284 difference in temporal coverage of Period 2 in the two years (i.e., there were more warm days in Period 2
285 in 2020). Note that the hypothetical emissions in Period 2H are estimated based on the assumption of no
286 shutdown effects in both Period 1 and Period 3. Therefore the reduction of those pollutant emissions in
287 2020 might be even larger considering the lag effects of COVID-19.

288 **3.2 The shutdown effects on ambient concentrations**

289 Using the RSM, we predicted concentrations based on the updated emissions from the response-
290 based inversion model. In general, the simulated concentrations based on the adjusted emissions matched
291 well with the observed concentrations, as shown in Figure 4 for NCP averages and detailed by province
292 in Figure S1-12. More important, during the shutdown period in both years, the simualtions using adjusted
293 emissions without considering shutdown influcences significantly overestimate the NO_2 concentations in
294 2019 and 2020 by 61% and 81%, respectively. The high-biases in 2019 and 2020 are reduced to within 1%
295 in the simualtion with consideration of shutdown effects (Figure 4a). To evaluate the performance of
296 assimilation, we also conducted the cross valdiation by using 50% observation sites for estimating the
297 emission ratio which to be applied on the rest 50% observation sites for testing. The performance of cross
298 valdiation is exmained, suggesting quite similar results with that using all observation sites as shown in
299 Figure 4. The estimated percent changes in emissions due to the shutdown in Period 2 from cross-
300 validation are also close to that using all observation sites, as shown in Figure S13.

301 The results for O_3 are quite interesting, as simulated O_3 concentrations are close to observations in

both simulations with and without consideration of shutdown influcences (Figure 4b). The apparent insenstivity of O_3 concentrations to emission changes during the shutdown can be explained by the opposite response of O_3 to its two percurors, NO_x and VOC. In Figure 5a, we compare the response of O_3 concentrations for two NO_x and VOC emission change pathways starting from the hypothetical emissions for no-shutdown conditions (black symbol in Figure 5a). Since NO_x emissions clearly decreased due to the shutdown, the O_3 concentrations would increase if VOC emissions remained constant (following the green line to the green symbol in Figure 5a). Yet the simulation without consideration of VOC emission changes would result in a high bias of simulated O_3 concentrations compared to the observations by 49% in 2019 and 29% in 2020. The low observed O_3 concentrations during Period 2 in both years indicates that VOC emission reductions must have occurred to maintain the suppressed O_3 level (following the red line to the red symbol in Figure 5a). Consistent with this interpretation, the simulated O_3 concentrations agree well with observations (e.g., normarlized mean bias, NMB < 3%) when both NO_x and VOC emission reductions are represented.

The substantial reduction of NO_x emissions also resulted in noticable decreases in NO_3^- concentrations (black and green lines in Figure 4c). However, the low bias in NO_3^- predictions cannot be readily mitigated by adjusting the NH_3 emissions, because the substantial decreases in NO_x emissions associated with the shutdown result in strong NH_3-rich conditions, where NO_3^- concentrations are less sensitive to NH_3 emissions increases. The response of NO_3^- concentrations to pathways of NO_x and NH_3 emission changes is depicted in Figure 5b (SO_2 and VOC emissions are also changing simutaneously with NO_x). A larger decrease in simulated (from that with no consideration of shutdown influcences) than observed NO_3^- concentrations is associated with the NO_x emission reductions, but the change of NH_3 emissions can hardly increase the NO_3^- concentrations under such strong NH_3-rich conditions. Therefore, the model predicted no NH_3 changes in 2019, but very small increases of NH_3 emissions (+2%) in 2020 due to the increased activities in rural areas which slightly reduced the NO_3^- low biases (NMB from -12%

to -11%).

The large reduction in SO_2 emissions estimated with the response model during the 2020 shutdown considerably reduced the high biases in simulated SO_2 and SO_4^{2-} concentrations (Figure 4d-f). However, the SO_4^{2-} biases are still considerable after the emission adjustment because a large fraction of SO_4^{2-} might come from primary sources, which need further investigation especially for its contribution to p-$PM_{2.5}$.

Agreement between the simulated and observed $PM_{2.5}$ concentrations also improves when accounting for the reductions in primary $PM_{2.5}$ emissions estimated with the response model in both years (Figure 4g). Another interesting finding is that the simulated $PM_{2.5}$ concentrations with consideration of all emission changes due to the shutdown (red line in Figure 4g) are quite similar to $PM_{2.5}$ predictions without consideration of the shutdown impacts (black line in Figure 4g). The same behavior is evident for O_3 concentrations (red and black lines in Figure 4b). As discussed above, the reductions in emissions of multiple species during the shutdown had compensating influences on air quality, and the overall effects of the emission changes on O_3 and $PM_{2.5}$ concentrations were neutralized to a relatively small level.

3.3 Impacts of individual emission changes from the shutdown on O_3 and $PM_{2.5}$ concentrations

To further investigate the individual impacts of emission changes of each pollutant on O_3 and $PM_{2.5}$ concentrations, we conducted a sensitivity analysis by sequentially adding each incremental emission change into the model system and then calculating the associated changes in O_3 and $PM_{2.5}$ concentrations. By incrementally adding the impacts of emission changes of five pollutants (ΔNO_x, ΔVOC, ΔNH_3, ΔSO_2, and Δp-$PM_{2.5}$), the concentrations change from the original simulation, without consideration of shutdown impacts (noted as oSIM, shown as grey bar in Figure 6), and ultimately reaching observed levels (noted as OBS, shown as narrow blue bars in Figure 6). One thing should be noted that we scaled the individual impact of emission changes based on the ratio of observation to the adjusted simulation after considering overall impacts, to eliminate the small discrepancy between the observations and the adjusted simulations after considering the overall impacts. Therefore, the overall changes in concentrations due to the shutdown

can be reflected by the difference between the observation (OBS) and simulation with no consideration of shutdown (oSIM).

For O_3, the reduction of NO_x emissions lead to a significant enhancement of O_3 (see ΔNO_x) due to the VOC-limited regime in winter (Xing et al., 2019), while such O_3 enhancement has been largely or completely mitigated thanks to the simultaneous reduction of VOC emissions (see ΔVOC) in both 2019 and 2020. This behavior is particularly evident in Henan and Shandong provinces which experienced substantial VOC reductions during the shutdown (Table 3). Such benefits from simultaneous VOC controls also occurred for $PM_{2.5}$ concentrations. Compared with O_3, the changes in $PM_{2.5}$ concentrations are more complex to interpret due to the influence of emission changes for SO_2 (ΔSO_2), NH_3 (ΔNH_3) and p-$PM_{2.5}$ (Δp-$PM_{2.5}$) in addition to NO_x and VOC. Results suggest that the reductions of p-$PM_{2.5}$ emissions tended to favor $PM_{2.5}$ decreases while the ΔSO_2 and ΔNH_3 emission changes have negligible influence. Overall, reductions in p-$PM_{2.5}$ and VOC emissions helped mitigate potential $PM_{2.5}$ concentration enhancements in most NCP provinces. Similar findings are suggested in Hang et al. (2020), which observed enhanced secondary pollution during the COVID-19 period. The air quality impacts from the unexpected controls during the COVID-19 shutdown suggest that strengthened controls on p-$PM_{2.5}$ emissions and well-balanced reductions in NO_x and VOC emissions would be an effective strategy for further improving air quality in NCP (Xing et al., 2018).

4. Summary and Conclusion

In summary, this study developed a response-based inversion modeling framework and applied it to characterize the emission changes and associated air quality impacts during the 2019 Spring Festival and the 2020 COVID-19 pandemic shutdown. Our results indicate that the response model can effectively adjust the assumed prior emissions such that air quality predictions match well with observed concentrations. The model also captures the temporal variations of emissions associated with changes in meteorological conditions. The model may suffer some uncertainties from deficiencies in model chemical

mechanisms (e.g., conversion of SO_2 to SO_4^{2-}), as well as the quality of prior emissions and limited coverage of observations. Difficulties are also found in estimating the NH_3 emission changes under strong NH_3-rich conditions by using the current inversion method based on the concentration of PM chemical components. However, with the continued growth in observational datasets from both surface monitors and satellite retrievals, improvements in knowledge of atmospheric science, and development of advanced assimilation technologies, the new response-based inversion model has great potential to further improve the accuracy and efficiency of emission inventory updates. The importance of reliable bottom-up inventories for defining prior emissions by sector, combined with the ability of the top-down inversion model to rapidly adjust emissions for consistency with observations, demonstrates how bottom-up and top-down emissions modeling methods are complementary.

The response model was applied to the investigation of emission changes during the COVID-19 shutdown. The emission changes were estimated by comparing emissions for actual conditions with emissions for hypothetical conditions assuming that the shutdown did not occur. Emission levels during the COVID-19 shutdown period were estimated by applying the temporal profiles of sectoral emissions from the bottom-up inventory. These estimates may suffer some uncertainties associated with the temporal profiles and the assumption of no shutdown impacts during the post-shutdown period. Our results suggest that the shutdowns in 2019 and 2020 had considerable impacts on air pollutant emissions. Longer and stronger impacts are found in 2020 due to the COVID-19 pandemic compared to the Spring Festival of the previous year. The anthropogenic emissions of NO_2, SO_2, VOC, and primary $PM_{2.5}$ in NCP were reduced by 51%, 28%, 67% and 63%, respectively, due to the COVID-19 shutdown in 2020. The estimated ratio might be slightly underestimated considering the lag effects after the COVID-19 shutdown. We also found that emission changes associated with the shutdown periods had limited impacts on surface O_3 and $PM_{2.5}$ concentrations due to compensating effects of emission changes in different pollutants. Based on our analysis, careful controls on NO_x emission sources in NCP are recommended in combination with

simultanous controls on VOC and NH_3 sources. Such a comprehensive strategy would minimize the potential negative impacts on air quality of NO_x emission reductions during VOC-limited conditions in winter. This study also illustrates that air quality improvements do not necessary follow from precursor emission reductions, and multi-pollutant nonlinear response models are therefore critical tools for representing the nonlinear relationship between emissions and concentrations in designing effective control strategies.

Data and code availability

The original data and code used in this study are available upon request from the corresponding authors.

Author contribution

JX & SL designed the methodology, conducted the analysis, and wrote the original draft. YJ conducted the WRF-CMAQ simulation. SW & DD & ZD & JH helped with the bottom-up emission inventory. YZ helped with the RSM model. All authors contribute to writing the paper.

Acknowledgements

This work was supported in part by National Key R & D program of China (2018YFC0213805), and National Natural Science Foundation of China (21625701, 41907190). This work was completed on the "Explorer 100" cluster system of Tsinghua National Laboratory for Information Science and Technology. We thank Drs. Carey Jang, James Kelly, Jian Gao, and Jingnan Hu for contributions to the study. The authors gratefully acknowledge the free availability and use of observation datasets.

Competing interests

The authors declare no competing financial interests.

Reference

Cao, H., Fu, T.-M., Zhang, L., Henze, D. K., Miller, C. C., Lerot, C., Abad, G. G., De Smedt, I., Zhang, Q., van Roozendael, M., Hendrick, F., Chance, K., Li, J., Zheng, J., and Zhao, Y.: Adjoint inversion of Chinese non-methane volatile organic compound emissions using space-based observations of formaldehyde and glyoxal, Atmos. Chem. Phys., 18, 15017–15046, https://doi.org/10.5194/acp-18-15017-2018, 2018.

Ding, D., Xing, J., Wang, S., Liu, K., & Hao, J. (2019). Estimated contributions of emissions controls, meteorological factors, population growth, and changes in baseline mortality to reductions in ambient PM 2.5 and PM 2.5-related mortality in China, 2013–2017. Environmental health perspectives, 127(6), 067009.

Hartley, D., & Prinn, R. (1993). Feasibility of determining surface emissions of trace gases using an inverse method in a three-dimensional chemical transport model. Journal of Geophysical Research: Atmospheres, 98(D3), 5183-5197.

Huang, X., Ding, A., Gao, J., Zheng, B., Zhou, D., Qi, X., ... & Wang, J. (2020). Enhanced secondary pollution offset reduction of primary emissions during COVID-19 lockdown in China.

Li, L, et al. "Air quality changes during the COVID-19 lockdown over the Yangtze River Delta Region: An insight into the impact of human activity pattern changes on air pollution variation." Science of The Total Environment (2020): 139282.

Li, M., Zhang, Q., Kurokawa, J. I., Woo, J. H., He, K., Lu, Z., ... & Cheng, Y. (2017). MIX: a mosaic Asian anthropogenic emission inventory under the international collaboration framework of the MICS-Asia and HTAP. Atmospheric Chemistry and Physics (Online), 17(2).

Lu, Z., Streets, D. G., de Foy, B., Lamsal, L. N., Duncan, B. N., and Xing, J.: Emissions of nitrogen oxides from US urban areas: estimation from Ozone Monitoring Instrument retrievals for 2005–2014, Atmos. Chem. Phys., 15, 10367–10383, https://doi.org/10.5194/acp-15-10367-2015, 2015.

Mendoza-Dominguez, A., & Russell, A. G. (2000). Iterative inverse modeling and direct sensitivity analysis of a photochemical air quality model. Environmental science & technology, 34(23), 4974-4981.

Miyazaki, K., Eskes, H., Sudo, K., Boersma, K. F., Bowman, K., and Kanaya, Y.: Decadal changes in global surface NOx emissions from multi-constituent satellite data assimilation, Atmos. Chem. Phys., 17, 807-837, https://dx.doi.org/doi:10.5194/acp-17-807-2017, 2017.

Napelenok, S. L., Pinder, R. W., Gilliland, A. B., & Martin, R. V. (2008). A method for evaluating spatially-resolved NO x emissions using Kalman filter inversion, direct sensitivities, and space-based NO 2 observations.

Shi, X., Brasseur, G.P.: The Response in Air Quality to the Reduction of Chinese Economic Activities during the COVID-19 Outbreak, Geophysical Research Letters, 2020.

Tang, W., Arellano, A. F., Gaubert, B., Miyazaki, K., and Worden, H. M.: Satellite data reveal a common combustion emission pathway for major cities in China, Atmos. Chem. Phys., 19, 4269-4288, https://doi.org/10.5194/acp-19-4269-2019, 2019.

Tang, W., Cohan, D. S., Lamsal, L. N., Xiao, X., and Zhou, W.: Inverse modeling of Texas NOx emissions using space-based and ground-based NO2 observations, Atmos. Chem. Phys., 13, 11005–11018, https://doi.org/10.5194/acp-13-11005-2013, 2013.

Wang, P., Chen, K., Zhu, S., Wang, P., & Zhang, H. (2020). Severe air pollution events not avoided by reduced anthropogenic activities during COVID-19 outbreak. Resources, Conservation and Recycling, 158, 104814.

Wang, S., Xing, J., Chatani, S., Hao, J., Klimont, Z., Cofala, J., & Amann, M. (2011). Verification of anthropogenic emissions of China by satellite and ground observations. Atmospheric Environment, 45(35), 6347-6358.

Wang, S., Xing, J., Jang, C., Zhu, Y., Fu, J. S., & Hao, J. (2011). Impact assessment of ammonia emissions on inorganic aerosols in East China using response surface modeling technique. Environmental science & technology, 45(21), 9293-9300.

Wang, S., Zhao, M., Xing, J., Wu, Y., Zhou, Y., Lei, Y., ... & Hao, J. (2010). Quantifying the air pollutants emission reduction during the 2008 Olympic Games in Beijing. Environmental science & technology, 44(7), 2490-2496.

Wang, Q., Su, M.: A preliminary assessment of the impact of COVID-19 on environment – A case study of China, Science of The Total Environment, 728, 2020

Xing, J., Wang, S. X., Jang, C., Zhu, Y., & Hao, J. M. (2011). Nonlinear response of ozone to precursor emission changes in China: a modeling study using response surface methodology. Atmos. Chem. Phys, 11(10), 5027-5044.

Xing, J. P. J. M. R., Pleim, J., Mathur, R., Pouliot, G., Hogrefe, C., Gan, C. M., & Wei, C. (2013). Historical gaseous and primary aerosol emissions in the United States from 1990 to 2010. Atmospheric Chemistry & Physics, 13(15).

Xing, J., Wang, S., Zhao, B., Wu, W., Ding, D., Jang, C., ... & Hao, J. (2017). Quantifying nonlinear multiregional contributions to ozone and fine particles using an updated response surface modeling technique. Environmental science & technology, 51(20), 11788-11798.

Xing, J., Ding, D., Wang, S., Zhao, B., Jang, C., Wu, W., ... & Hao, J. (2018). Quantification of the enhanced effectiveness of NO x control from simultaneous reductions of VOC and NH 3 for reducing air pollution in the Beijing–Tianjin–Hebei region, China. Atmospheric Chemistry and Physics, 18(11), 7799-7814.

Xing, J., Ding, D., Wang, S., Dong, Z., Kelly, J. T., Jang, C., ... & Hao, J. (2019). Development and application of observable response indicators for design of an effective ozone and fine-particle pollution control strategy in China. Atmospheric Chemistry and Physics, 19(21), 13627-13646.

Xing, J., Zheng, S., Ding, D., Kelly, J. T., Wang, S., Li, S., ... & Zhu, Y. (2020). Deep learning for prediction of the air quality response to emission changes. Environmental science & technology, 54(14), 8589-8600.

Xing et al., Data assimilation of ambient concentrations of multiple air pollutants using an emission-concentration response modeling framework, under review

Zhang, L., Chen, Y., Zhao, Y., Henze, D. K., Zhu, L., Song, Y., ... & Huang, B. (2018). Agricultural ammonia emissions in China: reconciling bottom-up and top-down estimates, Atmos. Chem. Phys., 18, 339–355, 2018.

Zhang, S., Xing, J., Sarwar, G., Ge, Y., He, H., Duan, F., ... & Chu, B. (2019). Parameterization of heterogeneous reaction of SO2 to sulfate on dust with coexistence of NH3 and NO2 under different humidity conditions. Atmospheric environment, 208, 133-140.

Table 1 Sensitivity analysis for quantifying the impacts of individual pollutant emission changes on air quality

No.	Emission	Objective	Noted
Sim-1	All pollutants are used as the hypothetical emissions of Period 2H	To estimate the hypothetical concentrations without COVID impacts	oSIM
Sim-2	Same as Sim-1 except NO_x emissions are updated to actual emissions in Period 2	To estimate the impacts of NO_x emission changes on O_3 and $PM_{2.5}$ based on the difference between Sim-2 and Sim-1	ΔNO_x
Sim-3	Same as Sim-2 except VOC emissions are updated to actual emissions in Period 2	To estimate the impacts of VOC emission changes on O_3 and $PM_{2.5}$ based on the difference between Sim-3 and Sim-2	ΔVOC
Sim-4	Same as Sim-3 except NH_3 emissions are updated to actual emissions in Period 2	To estimate the impacts of NH_3 emission changes on $PM_{2.5}$ based on the difference between Sim-4 and Sim-3	ΔNH_3
Sim-5	Same as Sim-4 except SO_2 emissions are updated to actual emissions in Period 2	To estimate the impacts of SO_2 emission changes on $PM_{2.5}$ based on the difference between Sim-5 and Sim-4	ΔSO_2
Sim-6	Same as Sim-5 except primary $PM_{2.5}$ emissions are updated to actual emissions in Period 2	To estimate the impacts of primary $PM_{2.5}$ emission changes on $PM_{2.5}$ based on the difference between Sim-6 and Sim-5	Δp-$PM_{2.5}$

Table 2 Daily emissions of five pollutants in NCP provinces based on the response model (unit: kt/day)

2019	Period 1 (29 days, Jan 1 to Jan 29)					Period 2 (20 days, Jan 30 to Feb 18)					Period 3 (41 days, Feb 19 to Mar 31)				
	NO_x	SO_2	NH_3	VOC	p-$PM_{2.5}$	NO_x	SO_2	NH_3	VOC	p-$PM_{2.5}$	NO_x	SO_2	NH_3	VOC	p-$PM_{2.5}$
Beijing	0.49	0.07	0.20	0.69	0.12	0.26	0.05	0.19	0.20	0.01	0.48	0.05	0.23	0.94	0.16
Tianjin	0.65	0.17	0.15	0.92	0.05	0.42	0.17	0.15	0.24	0.04	0.79	0.21	0.25	1.37	0.15
Hebei	5.64	2.01	1.18	3.67	1.97	3.47	1.62	1.27	1.43	1.51	5.95	1.90	2.77	6.26	1.92
Shandong	7.35	3.21	1.34	8.58	0.76	4.45	2.88	1.52	2.41	0.88	6.90	3.45	3.54	9.59	1.19
Henan	5.34	1.49	1.31	4.08	1.54	3.04	1.31	1.74	0.71	1.84	4.46	1.84	4.27	4.46	1.33
NCP	19.47	6.96	4.17	17.94	4.43	11.65	6.03	4.87	5.00	4.28	18.58	7.45	11.07	22.62	4.76

2020	Period 1 (22 days, Jan 1 to Jan 22)					Period 2 (33 days, Jan 23 to Mar 5)					Period 3 (26 days, Mar 6 to Mar 31)				
	NO_x	SO_2	NH_3	VOC	p-$PM_{2.5}$	NO_x	SO_2	NH_3	VOC	p-$PM_{2.5}$	NO_x	SO_2	NH_3	VOC	p-$PM_{2.5}$
Beijing	0.38	0.04	0.20	0.65	0.01	0.23	0.03	0.20	0.27	0.01	0.28	0.04	0.24	0.70	0.09
Tianjin	0.64	0.12	0.15	0.87	0.02	0.44	0.12	0.17	0.44	0.03	0.71	0.18	0.30	1.20	0.10
Hebei	5.28	1.34	1.18	3.12	1.73	3.15	1.16	1.54	1.92	0.81	4.97	1.67	3.49	4.72	0.75
Shandong	6.57	2.55	1.34	8.02	0.85	3.28	2.25	1.88	2.44	0.16	5.87	3.57	4.52	8.44	0.14
Henan	4.50	1.15	1.31	3.84	2.26	1.13	1.14	1.31	0.64	0.16	4.09	2.13	5.49	3.13	0.10
NCP	17.37	5.19	4.17	16.51	4.88	8.23	4.69	5.10	5.71	1.17	15.93	7.59	14.03	18.18	1.19
Δ2020-2019	-11%	-25%	0%	-8%	10%	-29%	-22%	5%	14%	-73%	-14%	2%	27%	-20%	-75%

(p-$PM_{2.5}$ = primary $PM_{2.5}$)

Table 3 The shutdown-impacts on the emission of five pollutants in NCP provinces

2019	NO_x		SO_2		NH_3		VOC		p-$PM_{2.5}$	
	kt/Day	%	kt/Day	%	kt/Day	%	kt/Day	%	kt/Day	%
Beijing	-0.23	-47%	-0.01	-21%	0.00	0%	-0.56	-73%	-0.15	-93%
Tianjin	-0.30	-41%	-0.02	-10%	0.00	0%	-0.95	-80%	-0.07	-62%
Hebei	-2.33	-40%	-0.34	-17%	0.00	0%	-3.54	-71%	-0.51	-25%
Shandong	-2.67	-37%	-0.46	-14%	0.00	0%	-6.78	-74%	-0.10	-10%
Henan	-1.85	-38%	-0.48	-27%	0.00	0%	-3.39	-83%	0.39	27%
NCP	-7.38	-39%	-1.31	-18%	0.00	0%	-15.23	-75%	-0.43	-9%

2020	NO_x		SO_2		NH_3		VOC		p-$PM_{2.5}$	
	kt/Day	%	kt/Day	%	kt/Day	%	kt/Day	%	kt/Day	%
Beijing	-0.10	-30%	-0.01	-18%	0.00	2%	-0.39	-59%	-0.07	-85%
Tianjin	-0.24	-35%	-0.03	-18%	0.00	2%	-0.60	-58%	-0.04	-59%
Hebei	-1.98	-39%	-0.31	-21%	0.03	2%	-1.89	-50%	-0.43	-35%
Shandong	-2.95	-47%	-0.75	-25%	0.04	2%	-5.80	-70%	-0.31	-66%
Henan	-3.16	-74%	-0.76	-40%	0.03	2%	-3.10	-83%	-1.10	-87%
NCP	-8.42	-51%	-1.85	-28%	0.10	2%	-11.77	-67%	-1.95	-63%

(p-$PM_{2.5}$ = primary $PM_{2.5}$)

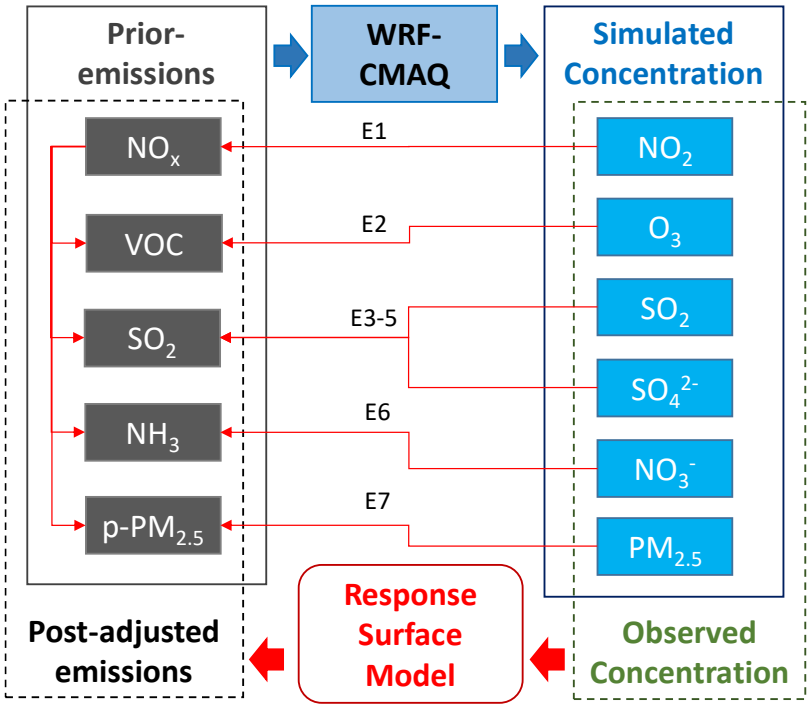

515

516 **Figure 1** The response modeling framework for adjusting the emissions (the E1-7 are equations used to
517 adjusted emissions, which are detailed in the text)

518

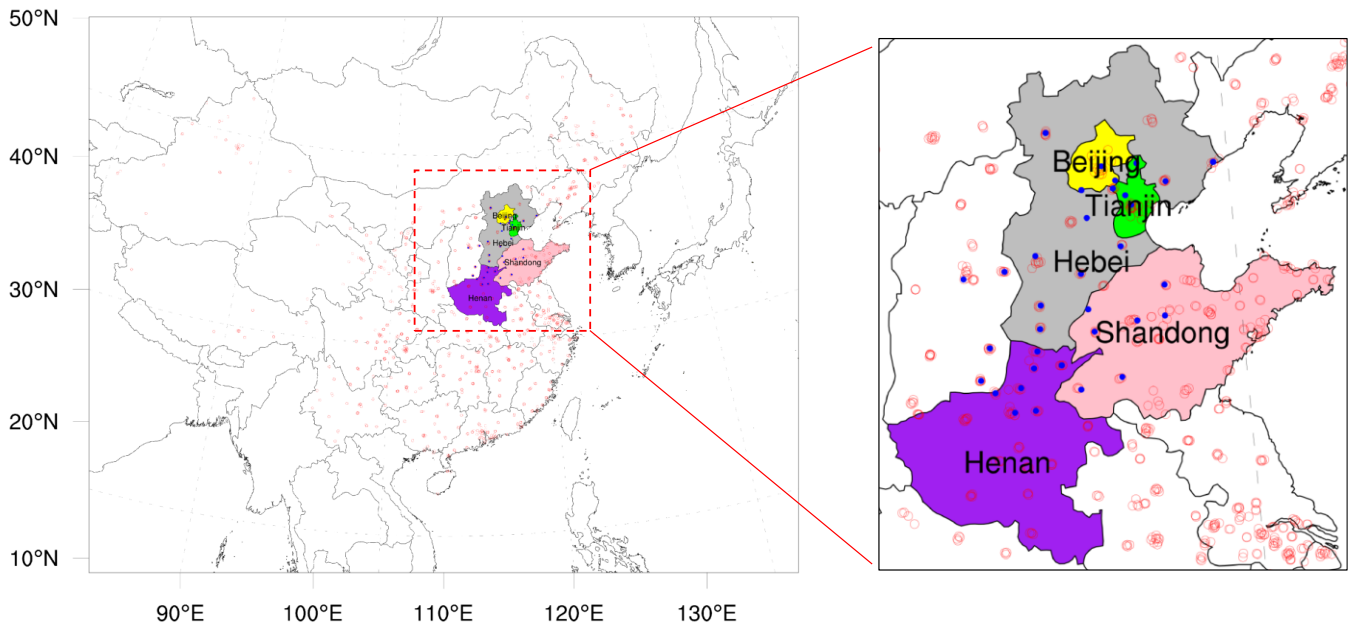

519

520 **Figure 2** Simulation domain and location of observation sites (colored area: five provinces of North
521 China Plain; red dots: surface monitor sites for NO_2, SO_2, O_3 and $PM_{2.5}$; blue dots: monitor sites for
522 $PM_{2.5}$ chemical compoments)

523

524

525

(a) 2019

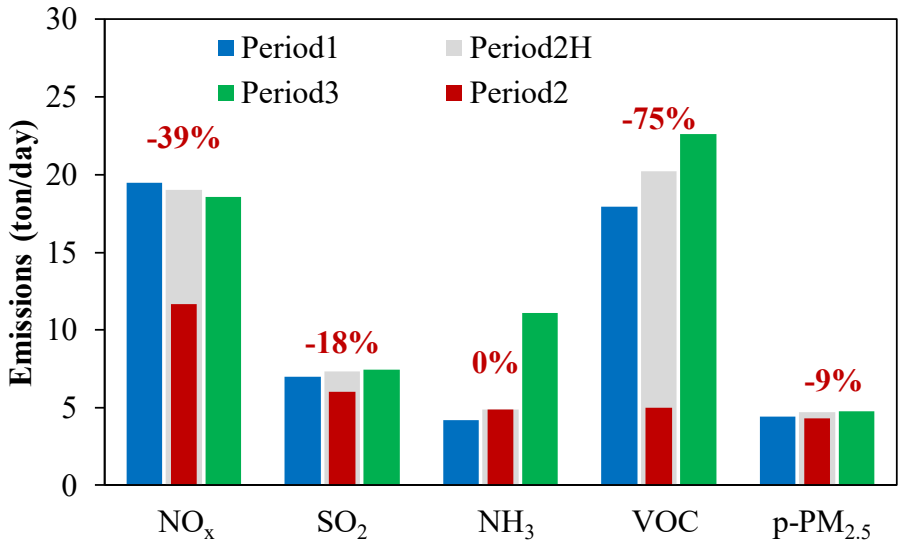

(b) 2020

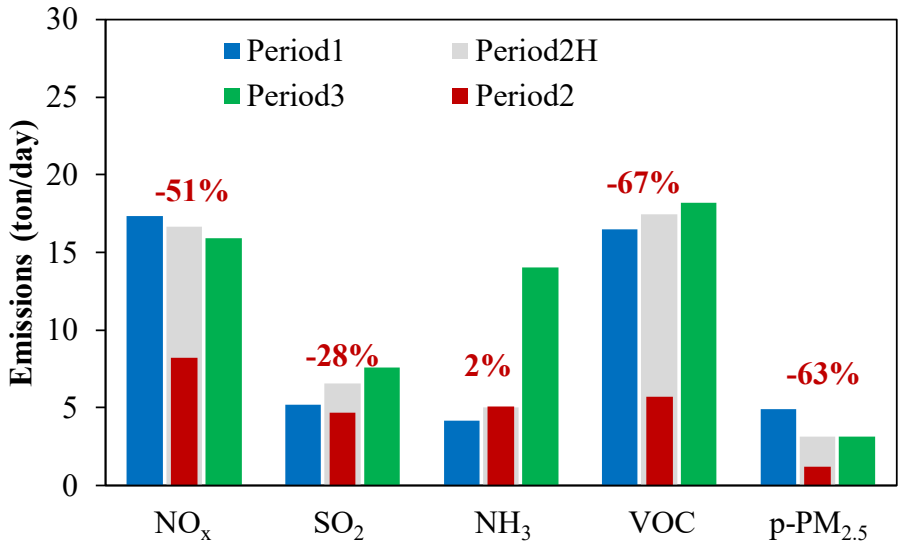

526 **Figure 3** Daily emissions during pre-shutdown (Period 1, blue), shutdown (Period 2, red), and post-
527 shutdown (Period 3, green) periods in 2019 and 2020. Period 2H (grey) is the hypothetical emissions
528 without reduced activity during the 2019 holiday or 2020 COVID-19 shutdown; the red number
529 indicates the percent change in emissions due to the shutdown in Period 2.

530

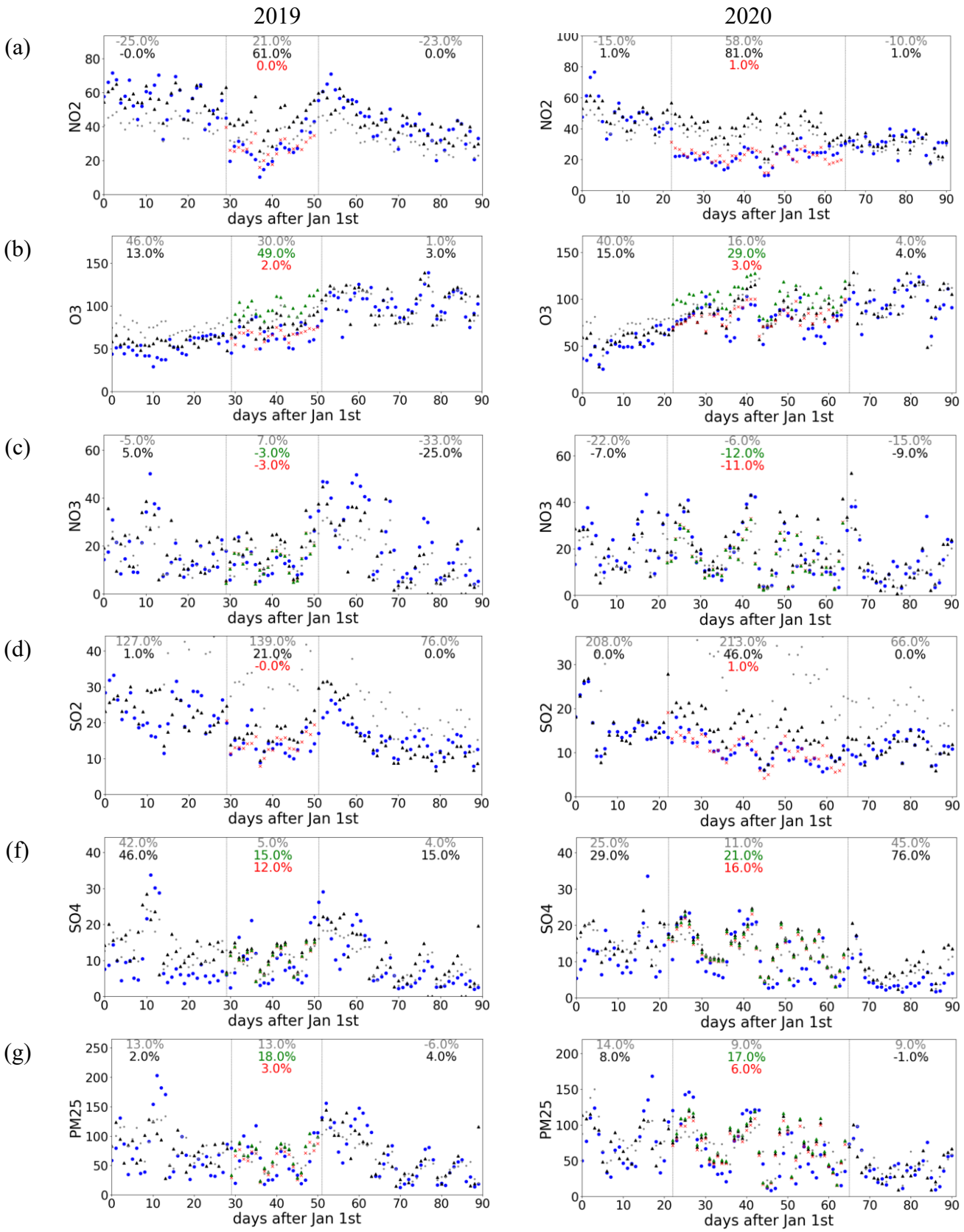

Figure 4 Comparison of the simulated and observed average concentrations in NCP (the percentage numbers indicate the normalized mean biases in hypothesis and actual simulations respectively for Period 2. Blue dots: observations; Black dots: simualtions using adjusted emission with no consideration

of shutdown influcences; Red dots : simualtions using adjusted emission with consideration of shutdown influcences; Green dots: simualtions using adjusted emission with consideration of shut-down influcences without VOC for O_3, NH_3 for NO_3^-, SO_2 for SO_4^{2-}, primary $PM_{2.5}$ for $PM_{2.5}$; Grey dots: orignal simualtion without assimilation; the regional average concentrations were calculated using spatially and temporally matched simulated and observed values; unit: $\mu g\ m^{-3}$)

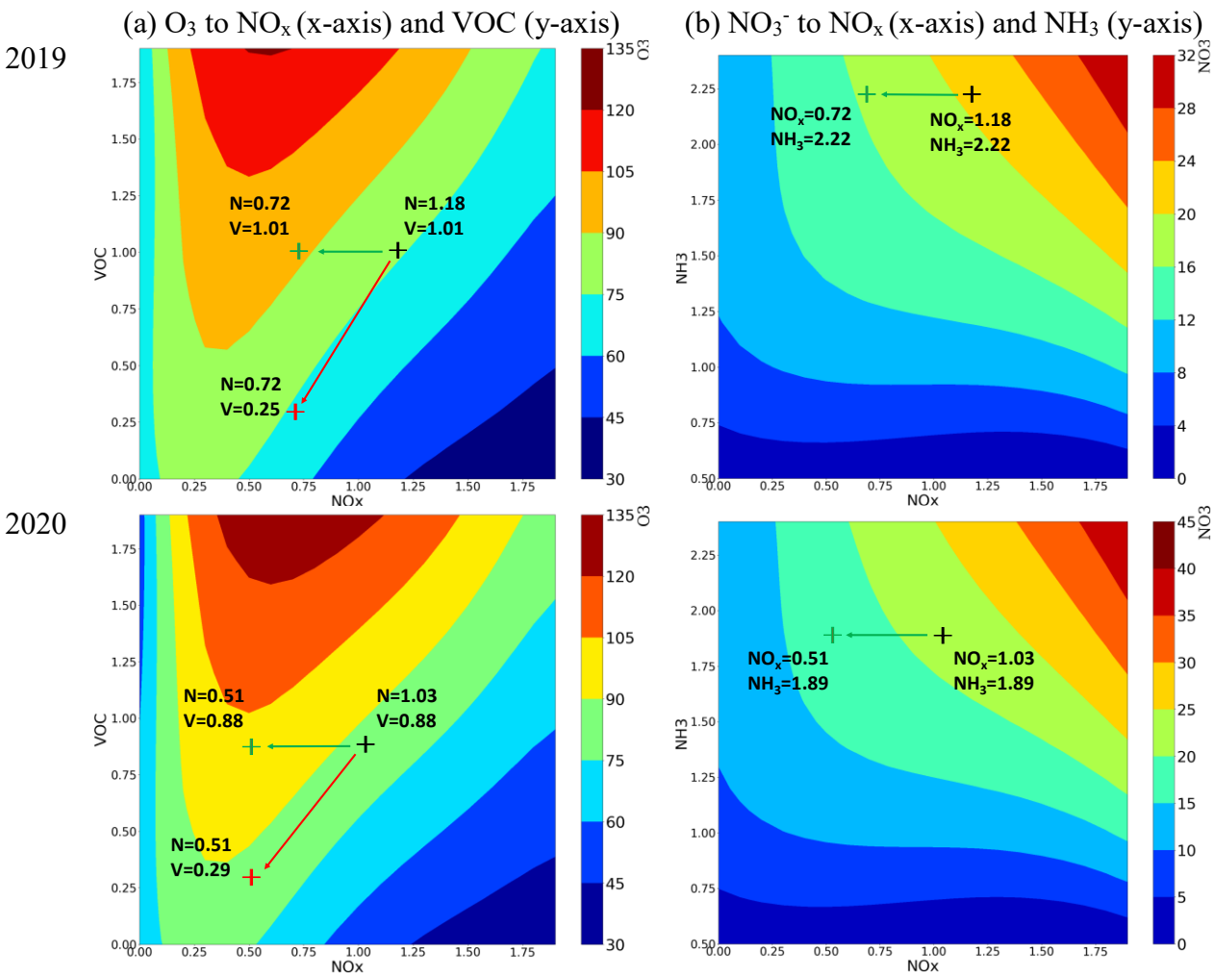

Figure 5 Implication of emission changes from the O_3 and NO_3^- response isopleths during shutdowns (the axes indicate emission ratios relative to the prior emissions; black symbol: adjusted emission ratios with no consideration of shutdown; red symbol: adjusted emission ratios with consideration of shutdown; green symbol: adjusted emission ratios without considering simutanous VOC changes for O_3, and NH_3 changes for NO_3; backgroud color: O_3 and NO_3^- concentrations, μg m^{-3})

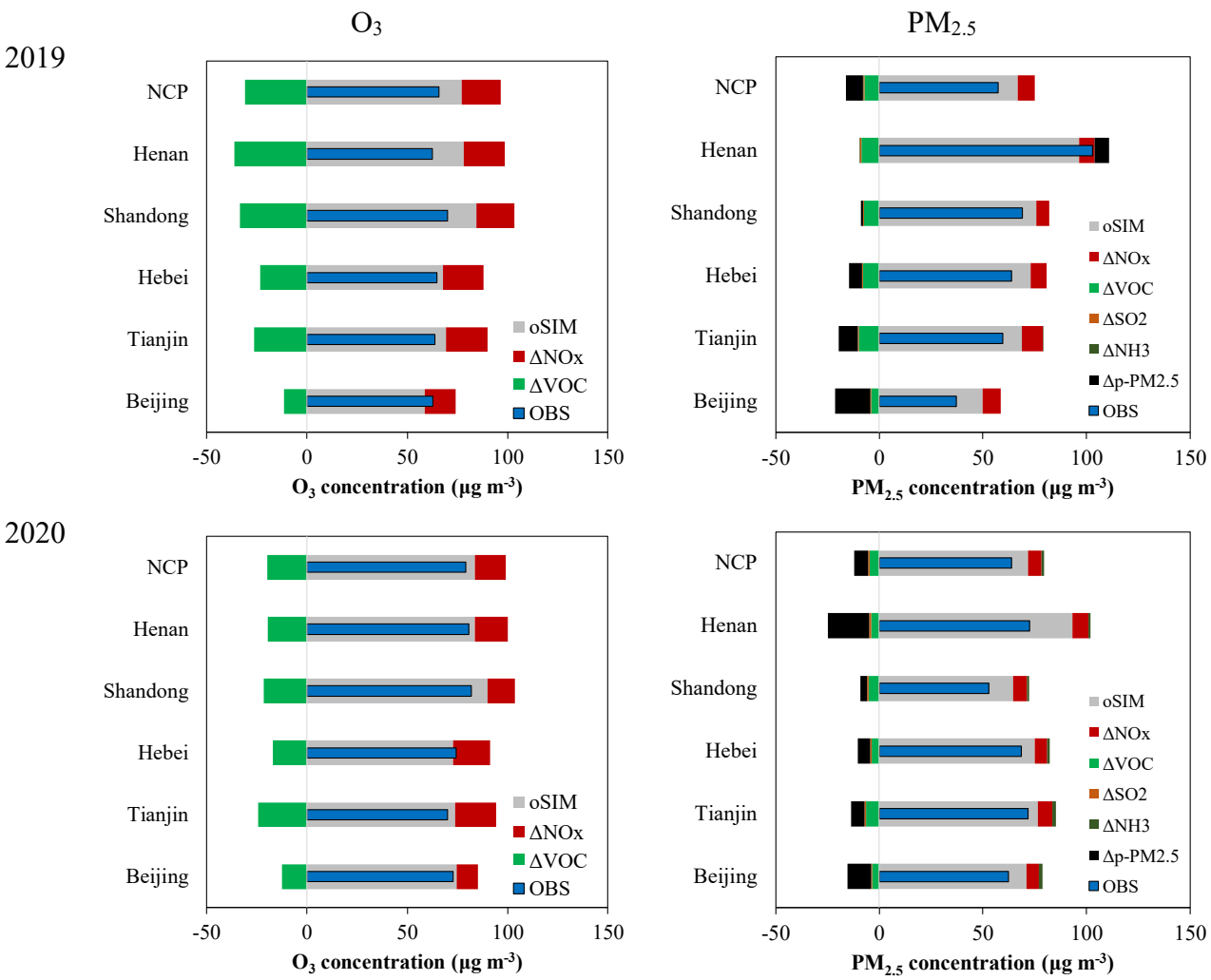

Figure 6 Contributions to the changes of O_3 and $PM_{2.5}$ concentrations during Period-2 (OBS: observation; oSIM: no consideration of shutdown; ΔNO_x: impacts due to the change of NO_x emissions; ΔVOC: impacts due to the change of VOC emissions; ΔNH_3: impacts due to the change of NH_3 emissions; ΔSO_2: impacts due to the change of SO_2 emissions; $\Delta p\text{-}PM_{2.5}$: impacts due to the change of primary $PM_{2.5}$ emissions)